Firing Fields of Dorsocaudal Medial Entorhinal Cortex as a Context-Independent Spatial Map

Erick Chastain Yanxi Liu

CMU-RI-TR-06-02

January 2006

Robotics Institute
Carnegie Mellon University
Pittsburgh, Pennsylvania 15213

Abstract

The firing fields of the ”grid cells” found in the rat dorsocaudal medial entorhinal cortex (dMEC) present a surprising pattern of context-independent regularity. We use computational means to analyze and validate the geometric and algebraic invariant properties of the firing fields, leading to a context invariant spatial map. Our method computes the specific symmetry group implicitly associated with the spatial map, and quantifies the regularity of the firing fields to achieve a symmetry-based clustering of two different types of “grid cells.” This quantified regularity makes spatial mapping more computationally efficient and suggests a way to use the dMEC firing patterns to estimate the probabilty of the rat being located at different points in the room. Finally, general properties of context-independent population codes are suggested. Namely, context-independent population codes gain robustness by introducing uncertainty and ambiguity.

Contents

1 Introduction

The rat hippocampus is implicated in spatial learning and mapping [12]. However, it is considered just a component of a distributed network [15] [19] which subtends the rat's ability to find its direction [22], position [13] , and distance from a self-selected "home base." The rat finds this home base after exploratory gathering of food pellets [25]. A key component of rodent navigation are "place cells" in hippocampus [12] [20], which show selective firing to the rat's position in the enclosure. These cells also are affected by external, or allothetic features of the environment [13] [14]. These place cells allow the rat to map its environment and infer its position by providing a metric and directionally-oriented representation of the enclosure [13]. A representation of the room which is both metric and directional is called a spatial map. Place representation is context-specific [21], and so is not truly effective in general navigation. It is hypothesized that a representation upstream of the rat hippocampus is context-independent and thus useful for general navigation in any environment [16] [15]. This is because the Hippocampus has place cells that change from room to room. General navigation, however, requires a more abstract map (a single map or multiple maps) that is not anchored to one environment. One potential possibility for such a map is the multi-peaked firing fields found in dorsocaudal medial entorhinal cortex (dMEC), which accurately represent the rat's position [4] in a regular grid [6]. This is in sharp contrast to place cells' one-peak firing fields. [13] We show that dMEC grid cells may be context-independent enough to be a candidate for this type of general spatial map.

2 Context-Independence of the Entorhinal Grids

To fully explore the grid cell representation, it is necessary to examine the conditions under which the dMEC grid remains invariant. That is, under what transformations (or symmetry group) is the dMEC grid approximately unchanged? A preliminary response is that the pattern has distinct 2D periodicity. To formally study the regularity of the dMEC grid, it is necessary to describe the geometry of the grid. This was done by Hafting et. al. [6] without referring to its symmetry group. The authors themselves concluded that the grid was a regular lattice by looking at the autocorrelelogram of each cell's firing field. The form of the regular lattice was hexagonal, with six peaks being equidistant from the central peak. Some very intriguing aspects of this lattice form are that its tiles are composed of equilateral triangles [6] and the angular separation of the inner vertices of the hexagon is always a multiple of 60 degrees [6]. To further investigate the structure of the hexagonal grid, we apply an algorithm to recover the actual lattice structure of the grid on eleven different cells measured in parallel from a rat navigating a two-meter diameter circular enclosure (from the Hafting et. al [6] paper by communication with the authors). We compute the lattice structure of the firing field, and its symmetry (wallpaper) group. This allows us to learn under which transformations the spatial map is invariant. Also, we find the nearest regular lattice to quantify the regularity of the firing field microstructure. Finally, we demonstrate that grid cell representations form a valid spatial map which can be used for path-integration. Specifically, we construct a model of how the firing field lattice is both directional and has a

defined distance metric.

2.1 Microstructure of the Entorhinal Grid

A symmetry g of a geometric set S is a distance-preserving transformation that keeps S setwise invariant (ie g(S) = S). All symmetries of S form a group G [1] and is called the symmetry group of S. Thus the symmetry group of a grid cell lattice is a collection of all transformations which leave the grid cell representation invariant. Each transformation in the group is invertible and transformation composition is associative. There also exists an identity transformation, and most importantly any transformation in the group can be written in terms of the composition of two other transformations in the group [1]. The grid cell lattice is generated by a single tile. This tile can be translated in 2D such that it produces a *covering* (no gaps) and a *packing* (no overlaps) of the plane [5]. There are only five unit lattice shapes, which can generate all possible 2D lattice forms [1].

It has been remarked (see Fyhn et al. [4]) that the firing fields deviate from geometric and photometric regularity. This is what Liu et al. call a "near-regular texture" [9]. To quantify the amount of deviation from regularity, Liu et al. have devised a taxonomy of near-regular textures. A Type I near-regular texture has geometric regularity but lacks photometric (color/amplitude) regularity. A Type II texture has less regular geometry and more photometric regularity. A Type III texture has even less geometric regularity and photometric regularity than the other two types [9] (see Figure 1). More formal definitions are used for analysis of images, and are as follows. The equation for the geometric regularity **G** of the lattice is

$$\mathbf{G} = \sum_{i=1}^{N_i} \frac{(l_i - ||T_1||)^2}{||T_1||^2} + \sum_{j=1}^{N_j} \frac{(l_j - ||T_2||)^2}{||T_2||^2} + \sum_{k=1}^{N_k} \frac{(l_k - ||T_1 + T_2||)^2}{||T_1 + T_2||^2} + \sum_{m=1}^{N_m} \frac{(l_m - ||T_1 - T_2||)^2}{||T_1 - T_2||^2} \tag{1}$$

where l_i, l_j, l_k, and l_m are the lengths of the links in the lattice D_L corresponding to links in the regular lattice R_L along the directions of T_1, T_2, $T_1 + T_2$, and $T_1 - T_2$, respectively. N_i, N_j, N_k , N_m are the total number of links in D_L, and θ is the angle between T_1 and T_2 [9]. Vectors T_1 and T_2 form the boundary of a generating tile and can be used to generate the entire lattice (Figure 2).

The appearance regularity **A** is the average standard deviation of all corresponding pixels in all lattice tiles. Regular textures have $G = 0$ and $A = 0$. Type I textures have **G** close to zero and $A > 0$. Type II textures have $G > 0$ and **A** closer to zero. Type III textures have **G** and **A** scores much further from zero. [9]

Geometric regularity is inversely proportional to the texture's distortion (from a regular texture). If we fit a lattice structure onto the texture, the value **G** depends on the amount we must deform this lattice in order to make it fit the nearest regular pattern.

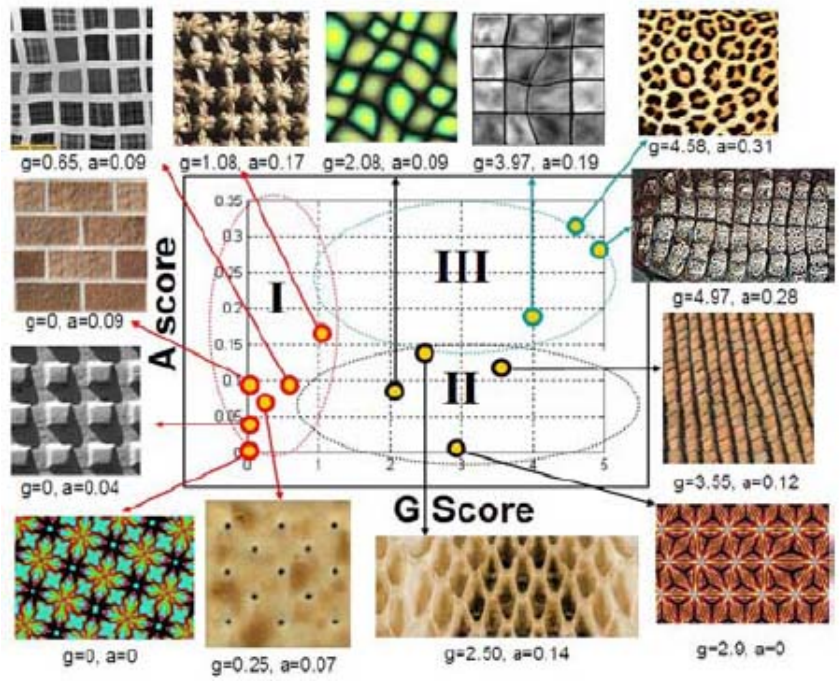

Figure 1: This figure from Liu et al. [9] illustrates examples of Type I, II, and III near-regular textures.

Photometric or appearance regularity can be thought of as quantifying the differences in amplitude of the peaks in the firing field. A Type II grid cell is more regular than a Type III grid cell, in the sense that the distance of the grid cell lattice from a regular lattice is smaller for Type II cells. This algorithm computes the nearest regular lattice implied by the texture. The algorithm takes a user-specified lattice D_L. Using D_L, the algorithm finds the nearest regular lattice via optimization using this formula:

$$min_{||T_1||,||T_2||,\theta}(\sum_{i=1}^{N_i}(l_i-||T_1||)^2+\sum_{j=1}^{N_j}(l_j-||T_2||)^2+\sum_{k=1}^{N_k}(l_k-||T_1+T_2||)^2+\sum_{m=1}^{N_m}(l_m-||T_1-T_2||)^2)$$

With all of the symbols being identical to those defined for the geometric regularity measure (Equation 1). Similar models are used in [23]. To deform each image pixel to fit the nearest regular lattice R_L, one needs to use the multilevel free-form deformation (MFFD) algorithm proposed in Lee et al. [8].

The results of using this analysis on the firing fields are illustrated in Figure 2. To the left (in Figure 2) is the original lattice, fitted by hand using the same user interface that was used by Liu et al. [9]. To the right (in Figure 2) is the regularized lattice, with image pixels morphed accordingly. The figure shows three of the eleven lattices fitted using this algorithm.

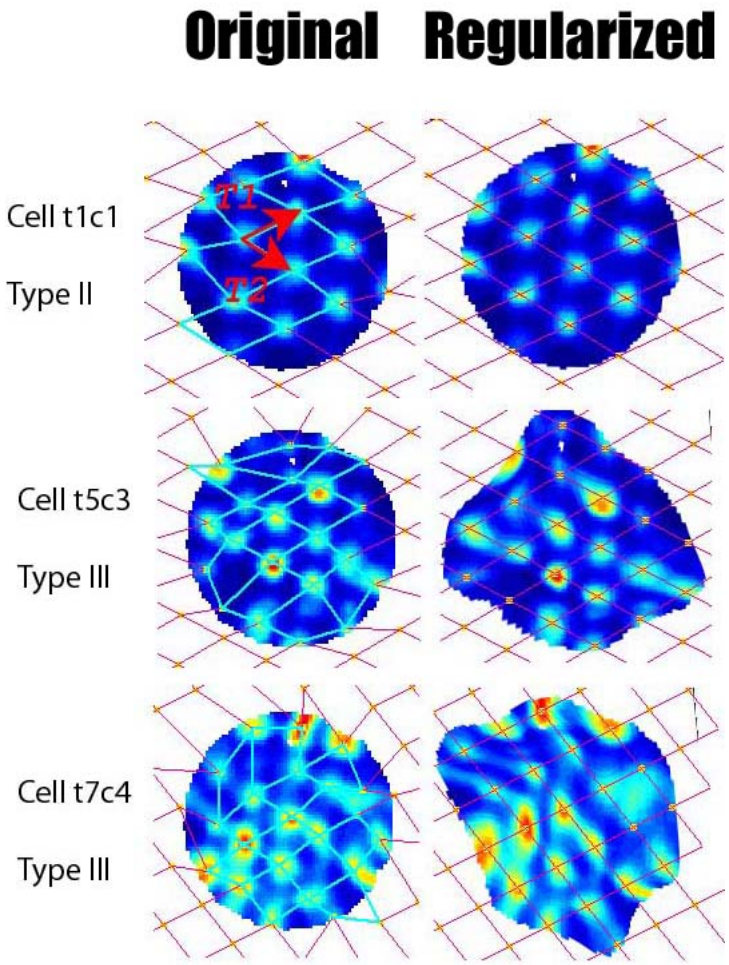

Figure 2: These are the firing fields of three different grid cells. The generating vectors T_1 and T_2 are indicated in red, the original firing pattern with its deformed lattice is on the left, and the nearest regular lattice is on the right. The regularized lattice is overlayed onto a morphed version of the image deformed to fit the lattice.

2.2 Regularity Quantification of Grid Cells

If we compute the **G** and **A** scores for all eleven of the grid cell lattices, they form two clusters, with centroids at positions $(8.6492, 0.1962)$ and $(2.2040, .1503)$ respectively. The first number is the **G** score and the second is the **A** score (see Figure 3). In Liu's classification of near-regular textures, the two clusters fall squarely within type II and III textures. Firing field lattices of type II are significantly more geometrically regular than that of the type III, but both have the same hexagonal lattice topology. Grid cells show variability between cell firing fields in both orientation and inter-peak spacing [6].

Instead of integrating over all different grid cells, a representative grid cell of each type can be used. This limits substantially the variability in spacing. Then, to account for the variability of orientation between grids, these representatives are rotated by different degrees and integrated. This ensures that all orientations of the grids are integrated over. Thus it is computationally efficient to represent the rat's position when integrating information from multiple cells. In fact, if we make a simplifying assumption and state that the representative cells are only rotated by 15, 30, and 45 degrees, then we will integrate over the firing fields of $3^2 = 9$ grid cells. Thus we hypothesize that grid cells can represent the rat's position by integrating the firings of just a few cells. This observation is mirrored by Fyhn et al. [4] and is stated explicitly as a hypothesis by Hafting et al. [6]. Fyhn et al.'s estimate of the number of neurons required to estimate position is eight [4], which is quite close to our estimate. If the variability of spacing was not restricted, the number of cells whose activity would have to be integrated is exponential in the number of distinct inter-peak distances.

2.3 Invariance properties of Grid Cell Firing Fields

The tile identified by Hafting et al. was an equilateral triangle, and the regularized lattices generated using our method agree with this model of the firing field lattice. The lattice tile actually contains two equilateral triangles. In addition, rotations of multiples of sixty degrees were identified to leave a vertex of the hexagonal tile approximately set-wise invariant (interpretation of what was said in Hafting et al.) [6]. The equilateral triangular tile is also captured by our regularized lattice recovered from the imaging data. Finally, given the regularized lattice of the grid cell firing fields, there is an approximate bilateral symmetry within a tile, even in the irregular type III examples of grid cells (see Figure 4). If we draw an axis which cuts the tile into two equilateral triangles, the part of the tile to the right of the axis is approximately equal to the left-hand side of the tile relative to the axis. There were some instances in which a single lattice point was missing, but this was uncommon enough that the underlying grid could still be said to have approximate bilateral symmetry along the axis described. An arbitrary lattice is defined by three points. This is only true if the lattice is *p6m*, for example.

The invariants just ascribed to grid cell representations suggest that dMEC lattices can be best fitted with the symmetry group *p6m*, one of the 17 symmetry groups for any 2D periodic pattern [17]. This makes the grid cell representation invariant under the most translations and rotations out of any possible regular tiling (mapping) of the enclosure [17]. A *p6m* lattice tile is shown in Figure 4. Translation and rotation of the firing field with respect to the center of the enclosure are caused by the rat's calibration of the grid cell firing to a small white rectangular (cue) card moving along the wall [6]. This suggests two major predictions about grid cell firing fields: grid cell firing is invariant under cue card rotations that are multiples of 60 or that cause changes in phase (translation) that are equal to linear combinations of T_1 and T_2 (whose mean lengths are from 39 to 73 cm for both vectors). This 60 degree rotational invariance could explain the observation by Hafting et al. that grid cells represent all orientations between 0 and 59

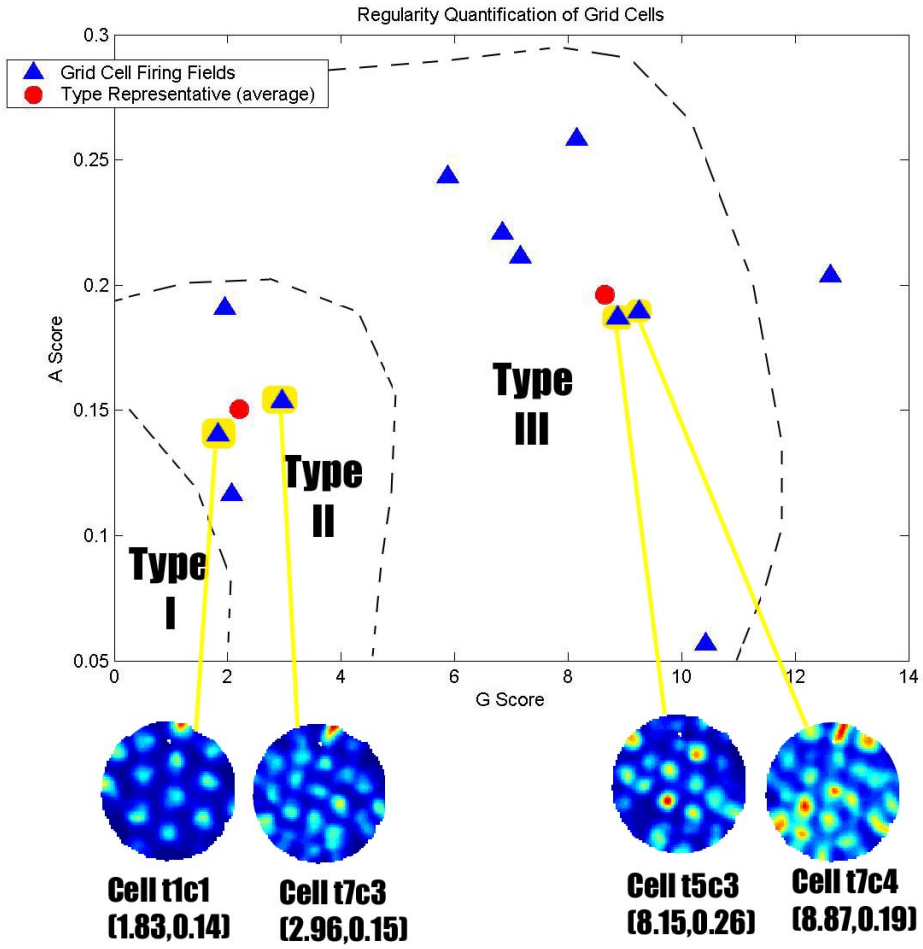

Figure 3: A plot of the **G** and **A** scores of all 11 grid cells fitted with regularized lattices. The first (leftmost) cluster of grid cells falls within type II Near-regular Lattices, and the second cluster of grid cells is of Type III, according to Liu's classification of Near-regular Lattices and Textures. [9]

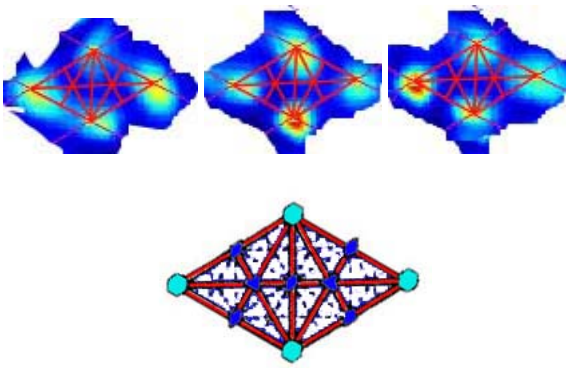

Figure 4: These are the first, fourth, and seventh tiles of cell t5c3 and the *p6m* tile. The three tiles from t5c3 are highly bilaterally symmetric, as can be seen by the similarity of both sides with respect to the axes demarcated by the red lines. A *p6m* tile has outer vertices that are invariant under 60 degree rotation, and is bilaterally symmetric along all of the solid lines. Diamonds signify invariance under 180 degree rotation around that point, and triangles signify invariance under 120 degree rotation around that point. All tiles have invariance under translations that are multiples of their generating vectors T_1 and T_2. What this signifies for the dMEC map is that it is invariant even under changes in the location of a small white rectangular (cue) card on the inside wall of the enclosure (rotations by multiples of 60 degrees). This is true because cue card rotation causes translation and rotation in grid cell firing [6]. This suggests a highly context-independent spatial map in dMEC grid cells.

degrees [6].

If it is indeed true that dMEC firing fields are invariant under 60 degree rotation, then we hypothesize that this allows the rat to not be tricked or distracted by (allothetic) sensory cues in the rat's environment which are all geometrically similar. In this case, if the multiple cues are separated by near-multiples of sixty degrees, only one of the cards should determine the orientation of the grid. Take for example hippocampal place cells under the influence of two cards that are 180 degrees apart. These place cells still have one peak in their firing field, which is tuned to the entry point of the rat [18]. Since 180 is a multiple of 60, perhaps the invariance of grid cell firing under 60 degree rotation contributes to this effect.

In addition to these invariants, there are many more, notably invariance under removal of the cue card (and darkness)[6], change of room [7], change of the scale of the enclosure [6], direction of movement [4], density [6], and novelty[6]. Our working hypothesis is that dMEC firing fields are more context-independent than head direction cells. This is because they are invariant under some degrees of external cue rotation (which is

not true of head direction cells, see Taube [22]), only one of the many invariances that a $p6m$ symmetry group implies. In any case, to have a general spatial map which can be used in many different environments is clearly valuable. Due to all of the invariances in the representation, it is quite possible that grid cells are the basis for this general spatial map.

3 Decoding the Rat's Position: A Neural Instantiation

The maximal invariance and quantified regularity of grid cell firing fields makes it possible to integrate over only a small number of cells. Integration over a few grid cells to find the rat's position is more important than it might at first seem. If it required integrating the activities of many grid cells, then the number of cells needed for decoding the rat's position from the dMEC population grows exponentially. If the number of cells required were truly this large, integrating over multiple cells to decode the rat's position would be biologically implausible. Invariance and the plausibility of integrating over multiple firing fields are directly proportional. This proportionality exists because if the invariance is too low, then the number of cells to integrate grows exponentially. If Invariance increases, however, then there is a decrease in the number of cells needed to decode position. However, if the number of cells integrated is too small, then discriminability of position decreases as well. This is the pitfall of having such a context-independent map: to discriminate position, multiple maps must be integrated.

Integrating over multiple maps to minimize ambiguity sounds very much like the practice of finding the marginalized predictive distribution, which integrates over all different possible probability distributions to find the probability of the rat being in one location given its path-so-far [11]. Thus one conjecture about the dMEC population code is that it represents a predictive probability distribution of the rat's position. The predictive distribution is merely the integration or sum of the information contributed by different grid cells. The predictive distribution is thus the total information about the rat's position.Each grid cell's information about the rat's position can be summarized nicely using a posterior distribution [2]. Because population codes have been implicated in the representation of posteriors [26] [27], and predictive distributions are proportional to the sum of posteriors, this gives a feasible neural instantiation of the predictive distribution. Thus, one potential neural implementation of the recovery of position from an ensemble of grid cells can be described in a similar fashion. Each grid cell encodes a posterior distribution quantifying that grid cell's contribution to information about the rat's position. Then all the posteriors are integrated via summation and this gives the predictive distribution of the rat's position.

4 Acknowledgments

Most of all, the first author wishes to acknowledge a very important course which opened the eyes of several students to the applications of Group Theory to analysis of images and encoding. This course, taught by Professor Liu, disabused the first author of

the notion that symmetry and group theory are too abstruse to be of any use. We would like to thank Torkel Hafting and Marianne Fyhn for their data and slides from the SFN meeting, and for answering their email expediently (quite a rare quality). Secondly, we would like to thank Dr. Wen-Chieh Lin and Chengyu Wu for their code and interface to find the near-regular lattices. Furthermore, the first author would like to thank Professor Dave Touretzky and Mark Fuhs for introducing him to the work of Marianne Fyhn and having preliminary discussions with him about work on an attractor network model of the Fyhn data. The first author would also like to thank Yama Thi Khuu, Vicente Malave, and David Seiler for very helpful discussions on this work.

References

[1] Coxeter, H.S.M. and Moser, W.O.J. Generators and Relations for Discrete Groups, 4th edn. (Springer-Verlag, New York, 1980).

[2] Duda, R., Hart, P., Stork, D. G. Pattern Classification, 2nd ed. (Wiley-Interscience, 2002)

[3] Etienne, A. S. & Jeffery, K. J. Path integration in mammals. Hippocampus 14, 180192 (2004).

[4] Fyhn, M., Molden, S., Witter, M. P., Moser, E. I. & Moser, M. B. Spatial representation in the entorhinal cortex. Science 305, 1258-1264 (2004).

[5] Grunbaum, B. and Shephard, G.C. Tilings and Patterns, (W.H. Freeman and Company, New York, 1987).

[6] Hafting, T., Fyhn, M., Molden, S., Moser, M., & Moser, E. I. Microstructure of a spatial map in the entorhinal cortex. Nature 436, 801-806 (2005).

[7] Hafting, T., By Communication.

[8] Lee, S., Chwa, K., Shin, S., & Wolberg, G. Image metamorphosis using snakes and free-form deformations. In Proceedings of ACM SIGGRAPH 1995, ACM Press / ACM SIGGRAPH, Computer Graphics Proceedings, Annual Conference Series, ACM, 439-448 (1995).

[9] Liu, Y., Lin, W. C. & Hays, J. Near-Regular Texture Analysis and Manipulation, SIGGRAPH, 2004.

[10] Liu, Y., Tsin, Y., & Lin, W. C. The Promise and Perils of Near-Regular Texture, International Journal of Computer Vision, 62, No. 1-2, 145-159. April, 2005.

[11] MacKay, D., Information Theory, Inference, & Learning Algorithms. (Cambridge University Press, 2002)

[12] OKeefe, J. & Nadel, L. The hippocampus as a Cognitive Map (Clarendon, Oxford, 1978).

[13] OKeefe, J. & Conway, D. H. Hippocampal place units in the freely moving rat: why they fire where they fire. Exp. Brain Res. 31, 573590 (1978).

[14] OKeefe, J. & Burgess, N. Geometric determinants of the place fields of hippocampal neurons. Nature 381, 425-428 (1996).

[15] Redish, A. D. Beyond the Cognitive Map: From Place Cells to Episodic Memory (MIT Press, Cambridge, 1999).

[16] Redish, A. D. & Touretzky, D. S. Cognitive maps beyond the hippocampus. hippocampus 7, 1535 (1997).

[17] Schattschneider, D., The Plane Symmetry Groups: Their Recognition and Notation, Am. Math. Monthly, 85, 439-450 (1978).

[18] Sharp, P. E., Kubie, J. L., & Muller, R. U. Firing properties of hippocampal neurons in a visually symmetrical environment: Contributions of multiple sensory cues and mnemonic processes. Journal of Neuroscience, 10, 9, 3093-3105.

[19] Sharp, P. E. Complimentary roles for hippocampal versus subicular/entorhinal place cells in coding place, context, and events. Hippocampus 9, 432443 (1999).

[20] Sharp, P. E. (ed.). The Neural Basis of Navigation: Evidence from Single Cell Recording. pp. vii-xxiii. (Kluwer Academic Publishers , 2002)

[21] Squire, L. R., Stark, C. E. & Clark, R. E. The medial temporal lobe. Annu. Rev. Neurosci. 27, 279306 (2004).

[22] Taube, J. S. Head direction cells and the neurophysiological basis for a sense of direction. Prog. Neurobiol. 55, 225-256 (1998).

[23] Terzopoulos, D., & Vasilescu, M. Sampling and reconstruction with adaptive meshes. IEEE Computer Vision and Pattern Recognition Conference, 70-75 (1991).

[24] Touretzky, D. S., Weisman, W. E., Fuhs, M. C., Skaggs, W. E., Fenton, A. A., and Muller R. U. Deforming the hippocampal map. Hippocampus 15,1,41-55 (2005)

[25] Whishaw, I. Q. & Brooks, B. L. Calibrating space: exploration is important for allothetic and idiothetic navigation. Hippocampus 9, 659-667, 1999.

[26] Zemel, R. “Cortical belief networks.” To appear in R. Hecht-Neilsen (Ed.): Theories of the Cerebral Cortex, 2000.

[27] Richard Zemel, Peter Dayan, and Alex Pouget. “Probabilistic interpretation of population codes.” Neural Computation, 10, 2, 403-430, 1998.